As soon as we understand the gentle slope of pressure P in Fig. 15.4, i.e., the right-hand side of Eq. (15.23), we will also understand the difference between the behaviors of energy and pressure, the left-hand side of Eq. (15.23), noted on comparing Fig. 15.3 with Fig. 15.5.

We will show, in section 16.2, that this non-ideal-gas behavior can be interpreted as resulting from perturbative quark–gluon interactions and the presence of the latent heat of the vacuum $\mathcal{B}$. An equivalent explanation invoking the presence of quasi-particles with mass, and quantum numbers of quarks and gluons, will also be considered.

16 Perturbative quark–gluon plasma

16.1 An interacting quark–gluon gas

As explained in section 14.1, the interactions between quarks and gluons are contained in the QCD Lagrangian Eq. (13.79), improved by gauge-fixing and FP-ghost terms Eq. (14.1). Strictly considered, the rules for Feynman diagrams we presented in Eqs. (14.2)–(14.8) are applicable to processes in perturbative vacuum, whereas to compute thermal properties of interacting quark and gluons, we are working in matter at finite temperature T and chemical potential μ. The generalization required is discussed in detail in the textbook by Kapusta [157].

A lot of effort in the past few decades has gone into the development of the perturbative expansion of the partition function. The series expansion, in terms of the QCD coupling constant g, has been carried out to order $[(g/(4\pi)]^5 = (\alpha_s/\pi)^{5/2}/32$ [282]. This series expansion, which was developed using as reference the perturbative vacuum in empty space, does not appear to lead to a convergent result for the range of temperatures of interest to us [36]: the thermodynamic properties vary widely from order to order, oscillating quite strongly around the Stefan–Boltzmann limit. It has therefore been claimed that the perturbative QCD thermal expansion has a zero-range convergence radius in α_s.

Our following considerations will be limited to the lowest-order perturbative term combined with the vacuum energy $\mathcal{B}$ and allow an excellent reproduction of the key features of lattice results. It remains to be understood why this is the case. It is not uncommon to encounter in a perturbative expansion a semi-convergent series. The issue then is how to establish a workable scheme. It is, for example, possible that a different scheme of perturbative approach, in which the QCD parameters (α_s and masses) are made nonperturbative functions of the medium using an in-medium renormalization group, would yield a better converging series in α_s.

Considering the inconclusive and rapidly evolving landscape of thermal

https://doi.org/10.1017/9781009290753.022 Published online by Cambridge University Press

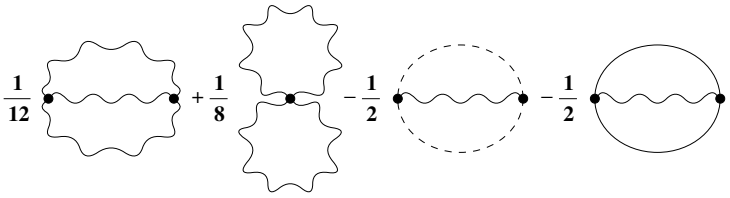

Fig. 16.1. Feynman diagrams contributing to the equation of state of the QGP in order α_s. Wavy lines represent gluons, solid lines represent quarks, and dashed lines denote the ghost subtractions of non-physical degrees of freedom.

QCD, we will in this book not explore the subject beyond the study of the consequences of the lowest-order thermal corrections. The lowest-order contributions are obtained by evaluating the graphs shown in Fig. 16.1. Evaluation of these diagrams at high temperature for massless quarks and gluons is possible analytically [91]. For massless quarks and antiquarks one finds the following two terms in the partition function:

$$\ln \mathcal{Z}_q(\beta,\lambda) = \frac{gV}{6\pi^2}\beta^{-3}\left[\left(1-\frac{2\alpha_s}{\pi}\right)\left(\frac{1}{4}\ln^4\lambda_q + \frac{\pi^2}{2}\ln^2\lambda_q\right) + \left(1-\frac{50\alpha_s}{21\pi}\right)\frac{7\pi^4}{60}\right], \tag{16.1}$$

where $g = n_s n_c n_f = 12$, for $n_s = 2s+1 = 2$, $n_c = 3$, and $n_f = 3$. The first term in parentheses is c_3, Eq. (4.71c), and the second is c_2, Eq. (4.71b). The quark fugacity λ_q is related to the baryon-number fugacity, as discussed in Eq. (11.3). The glue contribution is

$$\ln \mathcal{Z}_g(\beta,\lambda) = \frac{8\pi^2}{45}\beta^{-3}\left(1-\frac{15\alpha_s}{4\pi}\right), \tag{16.2}$$

where the last term in parentheses is c_1, Eq. (4.71a). Finally, the vacuum contribution can be added in the form

$$\ln \mathcal{Z}_{vac}(\beta) = -\beta\mathcal{B}V. \tag{16.3}$$

This term insures that the energy density, inside the bag, is positive and simultaneously that the pressure exerted on the surface of the bag is negative. The total grand partition function is

$$\ln \mathcal{Z}_{QGP} = \ln \mathcal{Z}_q + \ln \mathcal{Z}_g + \ln \mathcal{Z}_{vac}. \tag{16.4}$$

This equation was presented explicitly in section 4.6, Eq. (4.70). The resulting perturbative interactions between quarks and gluons are obtained by differentiating Eq. (16.4) with respect to V, β, and λ_q; see section 10.1.

Another important consequence of interactions in a conductive color plasma is the change in location of poles of particle propagators. Rather

https://doi.org/10.1017/9781009290753.022 Published online by Cambridge University Press

than of particles, one than speaks of quasi-particles, in our instance thermal quarks and gluons. The idea of quasi-particle thermal gluon and thermal quark masses is rooted in the desire to characterize, in a simple way, the behavior of quark and gluon correlators (propagators) evaluated inside the color-conductive medium. The monograph by Kapusta [157] offers an excellent early introduction to this still rapidly evolving subject, and we will restate here a few results of immediate interest.

Allowing for interaction to lowest order in $\alpha_{\rm s}$, a relation between the energy E and momentum $p = |\vec{p}|$ (a dispersion relation) of quasi-quarks is fixed by the location of the pole of the quark propagator Eq. (14.2) [270]:

$$E^2 = \vec{p}^{\,2} + (m_{\rm q}^{\rm T})^2 \left[\frac{E+p}{2p} - \frac{E^2-p^2}{4p^2} \ln\left(\frac{E+p}{E-p}\right)\right]. \tag{16.5}$$

For $p \to \infty$, with $E \to p + m^2/(2p)$, we recognize the quantity

$$\boxed{(m_{\rm q}^{\rm T})^2 = \frac{4\pi}{3}\alpha_{\rm s} T^2} \tag{16.6}$$

as the mass parameter, establishing the relation with the momentum and controlling the quasi-quark phase space.

Near to $p = 0$, the long-range oscillations described by Eq. (16.6) require more attention. They have the energy

$$E_{\rm q}(p \to 0) = \frac{m(\vec{p} \to 0, \omega; T)}{\sqrt{2}} + \frac{p}{3}\frac{\sqrt{2}p^2}{3m(\vec{p} \to 0, \omega; T)} + \cdots. \tag{16.7}$$

It is evident from the above that the 'thermal' mass of the quark in a medium may be defined also by considering this zero-momentum limit [270], rather than the high-momentum limit Eq. (16.6) adopted here. However, the domain $p \to 0$ is not important in the counting of states in the phase space, considering the momentum-volume factor $d^3p = 4\pi p^2\, dp$. We conclude that, in the study of the phase space of light thermal quarks in plasma, we should use for the light-quark energy the high momentum limit

$$E_{\rm q} \simeq \sqrt{p^2 + (m_{\rm q}^{\rm T})^2}, \quad {\rm q} = {\rm u}, {\rm d}.$$

A similar discussion arises for the behavior of gluons. The collective oscillations in the plasma with the quantum numbers of gluons behave, at high momentum, according to

$$E_{\rm g} \simeq \sqrt{p^2 + (m_{\rm g}^{\rm T})^2},$$

where

$$\boxed{(m_{\rm g}^{\rm T})^2 = 2\pi\alpha_{\rm s} T^2 \Big(1 + \frac{n_{\rm f}}{6}\Big),} \tag{16.8}$$

https://doi.org/10.1017/9781009290753.022 Published online by Cambridge University Press

whereas near $p \to 0$

$$E_{\rm g}(p \to 0) = \sqrt{\frac{2}{3}} m_{\rm g}^{\rm T}. \tag{16.9}$$

The thermal mass of gluons introduced in Eq. (16.8) is not the Debye screening mass limiting the effective range of interactions in plasma. This quantity corresponds to the static limit in the behavior of the longitudinal gluon-like plasma oscillations [269]:

$$\boxed{(m_{\rm g}^{\rm D})^2 = 4\pi\alpha_{\rm s} T^2 \Big(1 + \frac{n_{\rm f}}{6}\Big).} \tag{16.10}$$

16.2 The quark–gluon liquid

We consider the properties of the QGP allowing for the lowest-order interactions with a temperature-dependent interaction strength, and vacuum pressure $\mathcal{B}$. We refer to this model as the quark–gluon liquid [147]. Naturally, we hope and expect to reproduce lattice-QCD results [160]. There is considerable sensitivity to the value of $\alpha_{\rm s}(\mu)$ and it is necessary to use its precise form; see section 14.2.

Along with many other authors, we adopt the relation

$$\boxed{\mu \simeq 2\pi T} \tag{16.11}$$

between the scale of the QCD coupling constant and the temperature of the thermal bath. On the one hand, the right-hand side is close to the average collision energy of two massless quanta at T, and on the other, the relation Eq. (16.11) makes the thermal-QCD expansion least sensitive to the renormalization scale [283].

In Fig. 16.2, the 'experimental' values are the numerical lattice simulations [160], see section 15.5, for 2 (diamonds), 3 (triangles), and 2 + 1 (squares) flavors. The non-interacting Stefan–Boltzmann quark–gluon gas, Eq. (4.70), with $c_i = 1$ and with the bag constant

$$\mathcal{B} = 0.19\,{\rm GeVfm}^{-3} \tag{16.12}$$

is shown as thin lines, dotted for the case of three flavors and dashed for the case of two flavors. We see that the effect of vacuum pressure disappears as $T \to 2T_{\rm c}$, and that the lattice results differ significantly from those for the free gas, even at $T = 4T_{\rm c}$.

To obtain agreement with the lattice results, it is necessary to introduce perturbative coefficients c_i, Eqs. (4.71a)–(4.71c), with numerically computed $\alpha_{\rm s}(\mu = 2\pi T)$ [147]. The thick lines seen in Fig. 16.2 were obtained allowing for $\alpha_{\rm s}(2\pi T)$ shown in Fig. 14.3 with $T_{\rm c} = 160\,{\rm MeV}$. To find the behavior near to $T = T_{\rm c}$, the only 'free' choice we can make is

https://doi.org/10.1017/9781009290753.022 Published online by Cambridge University Press

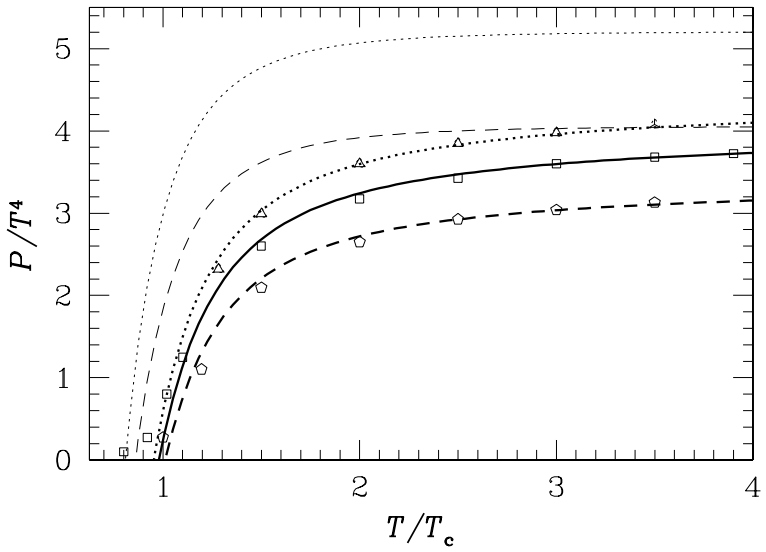

Fig. 16.2. Lattice-QCD results [160] for P/T^4 at $\lambda_q = 1$ (for 2 (diamonds), 3 (triangles), and 2 + 1 (squares) flavors) compared with free quark–gluon gas with bag pressure $\mathcal{B} = 0.19\,\mathrm{GeV\ fm}^{-3}$, thin dotted (three flavors) and dashed (two flavors) lines. Thick lines (agreeing with lattice data) are derived from the quark–gluon liquid model: dotted line, 3 flavors; solid line, 2 + 1 flavors; and dashed line, 2 flavors.

the value of $\mathcal{B}$, and this is the reason why that particular number was selected in Eq. (16.12). To achieve the agreement with lattice results seen in Fig. 16.2, the relevant relation is

$$\frac{\mathcal{B}}{T_c^4} = 2.2, \quad \mathcal{B}^{1/4} = 1.22 T_c. \tag{16.13}$$

The precise relationship between the scale μ and T has negligible impact on the result shown, as long as the natural order of magnitude seen in Eq. (16.11) is maintained. Within the simple model we introduced in section 1.3 to describe the phase transition, Eq. (16.13) implies nearly the correct number of degrees of freedom freezing in the transition, $\Delta g \simeq 20$.

It has been shown that it is also possible to reproduce the lattice results using fine-tuned thermal masses (see table I in [204]). In Fig. 16.3, we show the light-quark (solid thick line) and gluon (dashed thick line) thermal masses which were used to fit the lattice data. The actual thermal quark and gluon masses, defined in Eqs. (16.6) and (16.8), are also shown in Fig. 16.3, as thin lines (dashed for gluons) obtained using $\alpha_s(\mu = 2\pi T)$, from Fig. 14.3. We conclude that the thermal masses required to describe the reduction of the number of degrees of freedom for $T > 2T_c$ are

https://doi.org/10.1017/9781009290753.022 Published online by Cambridge University Press

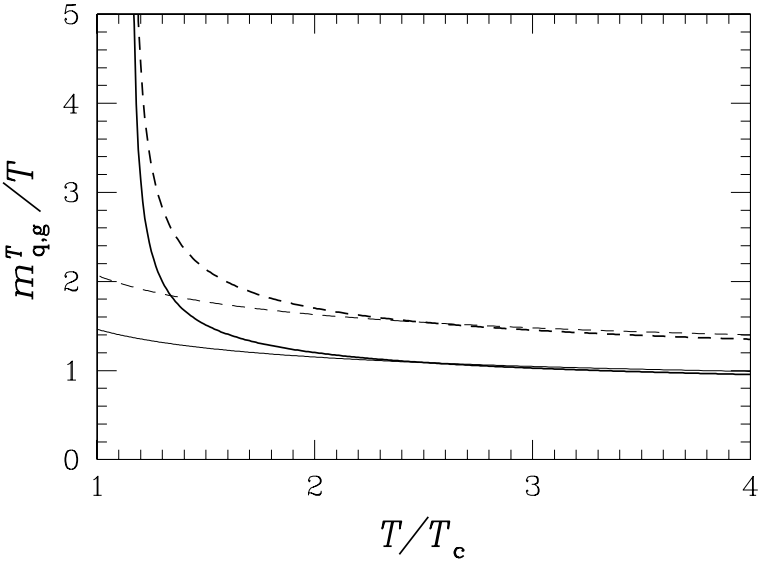

Fig. 16.3. Thermal masses fitted to reproduce lattice-QCD results for $n_f = 2$ [204], thick solid line for quarks, and thick dashed line for gluons. Thin lines, perturbative QCD result for $\alpha_s(\mu = 2\pi T)$.

just the perturbative QCD result. Importantly, this means that thermal masses express, in a different way, the effect of perturbative quantum-chromodynamics, and thus, for $T > 2T_c$, we have the option of using Eq. (16.1), or the more complex thermal-mass approach.

However, in the temperature domain $T < 2T_c$, in which the vacuum pressure $\mathcal{B}$ is relevant, see Fig. 16.2, the thermal mass required to fit lattice results, as can be seen in Fig. 16.3, is quite different from the perturbative QCD result, and we believe that the interpretation of lattice results in this phenomenologically important domain is much less natural than the quark–gluon-liquid approach. The introduction of thermal masses, in order to describe the behavior seen in Fig. 15.5, is expressing just the same fact that the pressure must be some function of the parameter Λ which is controlling the magnitude of the running α_s, and that additional physics, such as the vacuum pressure $\mathcal{B}$, is required in order to understand the behavior of the QGP, for $T < 2T_c$.

We have seen that the suppression of the number of degrees of freedom, seen in the QGP pressure can be well described by a first-order thermal QCD result, either using thermal masses, or more directly using the first-order corrections seen in Eqs. (16.1) and (16.2). However, to describe the behavior for $T \to T_c$, we should invoke nonperturbative properties of the vacuum. As discussed at the end of section 15.5, once the variation of

https://doi.org/10.1017/9781009290753.022 Published online by Cambridge University Press

P/T^4 with T has been described, the deviation of lattice results from the ideal-gas law, $\epsilon - 3P \to 0$, is also understood.

16.3 Finite baryon density

It is in the consideration of the finite baryon density that the issues regarding how to model the lattice results we raised in the last section are most relevant. We believe that it is appropriate to obtain the properties of QGP in a manner allowing the magnitude of the color interaction to be controlled by the energy scale which depends on the baryon-chemical potential. The dependence of the scale μ of α_s on the fugacity we adopt is [264]

$$\boxed{\mu = 2\sqrt{(\pi T)^2 + \mu_q^2} = 2\pi\beta^{-1}\sqrt{1 + \frac{1}{\pi^2}\ln^2\lambda_q}.} \tag{16.14}$$

Like with Eq. (16.11), there is no exact mathematical rationale for this expression; it is entirely based on intuition and the particle-energy behavior seen in studies of thermal QCD.

We note that Eq. (16.14) implies that

$$\begin{aligned} -\beta\,\frac{\partial\alpha_s(\beta,\lambda_q)}{\partial\beta} &= \mu\,\frac{\partial\alpha_s}{\partial\mu}, \\ \lambda_q\,\frac{\partial\alpha_s(\beta,\lambda_q)}{\partial\lambda_q} &= \frac{\ln\lambda_q}{\pi^2+\ln^2\lambda_q}\mu\,\frac{\partial\alpha_s}{\partial\mu}, \\ T\,\frac{\partial\alpha_s(T,\mu_q)}{\partial T} &= \frac{\pi^2T^2}{(\pi T)^2+\mu_q^2}\mu\,\frac{\partial\alpha_s}{\partial\mu}. \end{aligned} \tag{16.15}$$

The derivative of the QCD coupling constant can be expressed as, Eqs. (14.18) and (14.21),

$$\mu\,\frac{\partial\alpha_s}{\partial\mu} = -b_0\alpha_s^2 - b_1\alpha_s^3 + \cdots \equiv \beta_2^{\rm pert}. \tag{16.16}$$

$\beta_2^{\rm pert}$ is the beta-function of the renormalization group in the two-loop approximation, with b_i defined in Eq. (14.23). $\beta_2^{\rm pert}$ does not depend on the renormalization scheme, and solutions of Eq. (16.16) differ from higher-order results by less than the error introduced by the experimental uncertainty in the measured value of $\alpha_s(M_Z)$; see section 14.3.

https://doi.org/10.1017/9781009290753.022 Published online by Cambridge University Press

We are now prepared to study physical properties of the quark–gluon liquid. The energy density is obtained from Eq. (4.70):

$$\epsilon_{\rm QGP} = -\frac{\partial \ln \mathcal{Z}_{\rm QGP}(\beta,\lambda)}{V\,\partial\beta},$$
$$= 4\mathcal{B} + 3P_{\rm QGP} - \beta\,\frac{\partial\alpha_{\rm s}}{\partial\beta}\sum_{i=1}^{3}\frac{\partial c_i}{\partial\alpha}\,\frac{P_{\rm QGP}}{\partial c_i}. \tag{16.17}$$

We find that

$$\boxed{\epsilon_{\rm QGP} - 3P_{\rm QGP} = \mathcal{A} + 4\mathcal{B},} \tag{16.18}$$

where

$$\mathcal{A} = (b_0\alpha_{\rm s}^2 + b_1\alpha_{\rm s}^3)\left[\frac{2\pi}{3}T^4 + \frac{n_{\rm f}5\pi}{18}T^4 + \frac{n_{\rm f}}{\pi}\left(\mu_{\rm q}^2T^2 + \frac{1}{2\pi^2}\mu_{\rm q}^4\right)\right], \tag{16.19}$$

and $P_{\rm QGP}$ is stated explicitly in Eq. (4.70). We see in Eq. (16.18) the interesting property

$$\frac{\epsilon_{\rm QGP} - 3P_{\rm QGP}}{T^4} \to \frac{\pi}{18}(12 + 5n_{\rm f})(b_0\alpha_{\rm s}^2 + b_1\alpha_{\rm s}^3) + 4\frac{\mathcal{B}}{T^4},\ \mu_{\rm q} \to 0, \tag{16.20}$$

where the thermal interaction (the first term) is determining the behavior at $T \gtrsim 2T_{\rm c}$, Fig. 16.2.

A convenient way to obtain the entropy and baryon density uses the thermodynamic potential $\mathcal{F}$; see Eq. (4.70) and chapter 10. For the quark–gluon liquid, we have

$$\frac{\mathcal{F}(T,\mu_{\rm q},V)}{V} = -\frac{T}{V}\ln\mathcal{Z}(\beta,\lambda_{\rm q},V)_{\rm QGP} = -P_{\rm QGP}(T,\mu_{\rm q}), \tag{16.21}$$

with entropy density $s_{\rm QGP}$ and baryon density $\rho_{\rm b}$, which is a third of the quark density:

$$s_{\rm QGP} = -\frac{d\mathcal{F}}{V\,dT}, \quad \rho_{\rm b} = -\frac{1}{3}\frac{d\mathcal{F}}{V\,d\mu_{\rm q}}. \tag{16.22}$$

The entropy density is

$$\boxed{s_{\rm QGP} = \frac{32\pi^2}{45}c_1T^3 + n_{\rm f}\left(\frac{7\pi^2}{15}c_2T^3 + c_3\mu_{\rm q}^2T\right) + \mathcal{A}\frac{\pi^2T}{\pi^2T^2 + \mu_{\rm q}^2}.} \tag{16.23}$$

The coefficients c_i are defined in Eq. (4.71a) and are the same as in Eqs. (16.1), (16.2), and (4.70). The baryon density is

$$\boxed{\rho_{\rm b} = \frac{n_{\rm f}}{3}c_3\left(\mu_{\rm q}T^2 + \frac{1}{\pi^2}\mu_{\rm q}^3\right) + \frac{1}{3}\mathcal{A}\frac{\mu_{\rm q}}{\pi^2T^2 + \mu_{\rm q}^2}.} \tag{16.24}$$

https://doi.org/10.1017/9781009290753.022 Published online by Cambridge University Press

16.4 Properties of a quark–gluon liquid

The behavior of the quark–gluon liquid is of particular interest in the study of

- initial conditions corresponding to an early instant in time during the heavy-ion collision when the light quarks and gluons are in approximate chemical equilibrium, but strange quarks have not yet been produced, thus $n_f = 2$; and
- properties of the fireball of quarks and gluons at the time of its breakup near to $T = T_c$, at which strangeness is practically equilibrated, and $n_f = 2.5$.

Given the good agreement with the lattice results for vanishing chemical potential, the following study offers a quantitative description of the relationship between the temperature and physical properties reached in the deconfined phase, but with an unknown systematic error when properties involving baryon density are physically relevant (e.g., in the AGS energy range).

In the left-hand panels of Fig. 16.4, we show the physical properties at fixed energy per baryon, in the range $2\,\text{GeV} \leq E/b \leq 15\,\text{GeV}$, as functions of temperature, while in the right-hand panels we study the behavior at fixed value of the (dimensionless) entropy per baryon $10 \leq S/b \leq 60$. In panels (a) and (b) of Fig. 16.4, as we step from line to line from left to right, the energy per baryon is incremented by 1 GeV; in panels (d) and (e) the entropy per baryon is incremented by 5 units; in panel (c) we step from bottom to top incrementing by 1 GeV; and in panel (f) from bottom to top by 5 entropy units. The light-dashed boundaries are obtained from the conditions

- on energy density $\epsilon_{q,g} \geq 0.5\,\text{GeV fm}^{-3}$ (excluding here the latent heat of the vacuum $\mathcal{B} \simeq 0.19\,\text{GeV fm}^{-3}$), and/or
- baryochemical potential, $\mu_b \leq 1\,\text{GeV}$.

We highlight the result for $E/b = 8.5\,\text{GeV}$ by using a thick dashed line on the left in Fig. 16.4, and that for $S/b = 40$ by using a thick solid line on the right.

This systematic exploration should allow one to assess the behavior of the quark–gluon liquid possibly created in collisions performed in the energy range between those of the AGS and SPS accelerators, and comprising chemically equilibrated u and d quarks and gluons. The particle multiplicity in the final state tells us that the entropy per baryon is at the level of 40 units for the high-energy range of the SPS; see section 7.4. The corresponding temperature which we read from panel (c) for $E/b < 8.5$ GeV is $T < 280$ MeV. Evaluation of properties of the final abundances of particles, section 19.3, shows that it is easier to deposit baryon number

https://doi.org/10.1017/9781009290753.022 Published online by Cambridge University Press

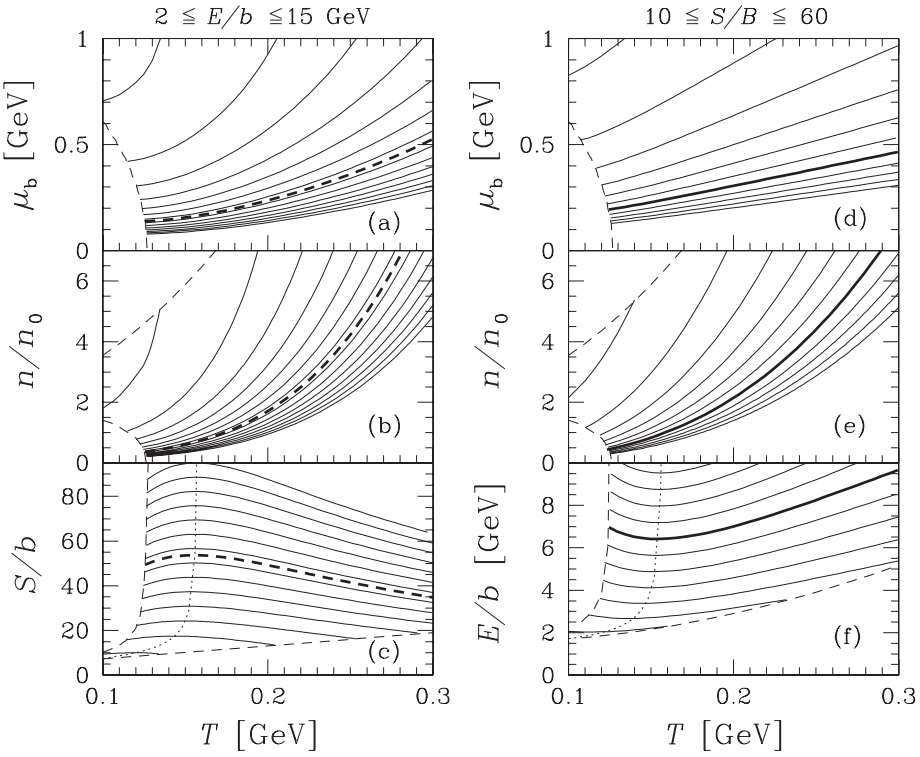

Fig. 16.4. Left: lines corresponding to fixed energy per baryon $E/b = 2$ to 15 GeV in steps of 1 GeV: (a) baryo-chemical potential $\mu_{\rm b}$ (highest E/b at the bottom), (b) baryon density n/n_0 in units of equilibrium nuclear density (highest E/b at the bottom), and (c) S/b, the entropy per baryon (highest E/b at the top). Right: lines corresponding to fixed entropy per baryon $S/b = 10$ to 60 in steps of 5, from top to bottom: (d) $\mu_{\rm b}$, (e) n/n_0, and (f) E/b; see the text for further details.

than energy in the fireball, and, in general, the initial energy per baryon is smaller than the collisional kinematic limit. Taking $E/b \simeq 7$ GeV, we obtain $T_{\rm ch} \simeq 220$. Before the light-quark flavor has been equilibrated, the temperature of gluons could be as high as $T_{\rm th} \simeq 250$ MeV, for the SPS top energy.

We see in Fig. 16.4 panels (a) and (d) the appropriate ranges of the baryo-chemical potential; and in panels (b) and (e) the baryon density in units of equilibrium nuclear density, $n_0 = 0.16$ fm^{-3}. The dotted lines in panels (c) and (d) show where $P_{\rm q,g} - \mathcal{B} = 0$: there, the entropy per baryon at fixed energy per baryon reaches its maximum as a function of temperature, and the energy per baryon at fixed entropy per baryon reaches its minimum. In an equilibrium transition, the QGP transforms

https://doi.org/10.1017/9781009290753.022 Published online by Cambridge University Press

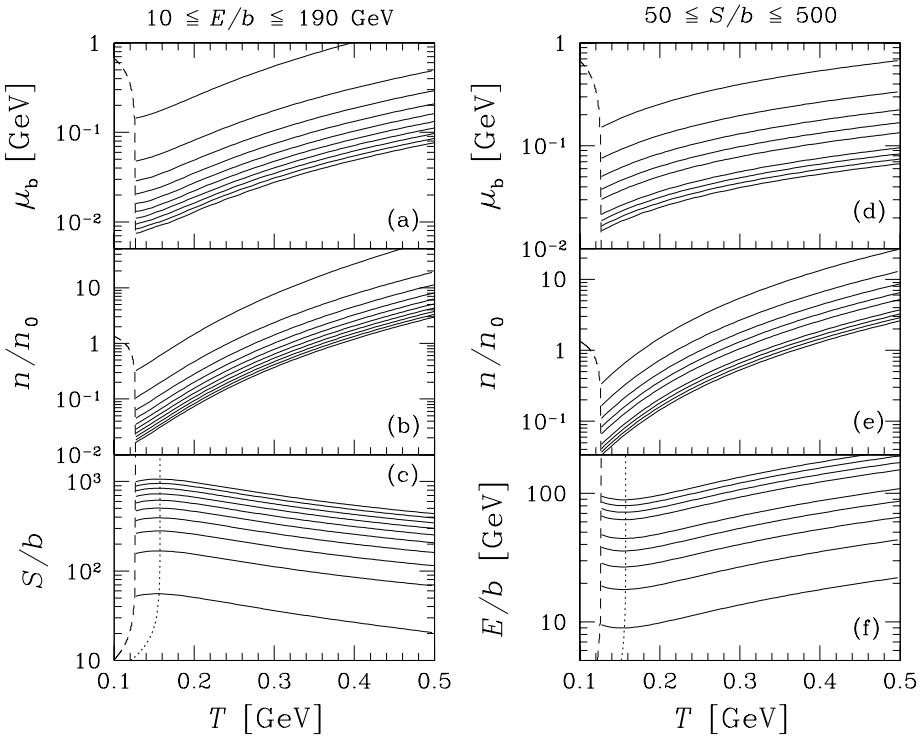

Fig. 16.5. The analog of Fig. 16.4 for the RHIC energy domain. Left, lines at fixed energy per baryon $E/b = 10$ to 190 GeV in steps of 20 GeV. Right, lines at fixed entropy per baryon $S/b = 50$ to 500 in steps of 50; see the text for more details.

for T above this condition, since the 'external' hadron pressure needs to be balanced. In an exploding system, the breakup occurs at T below this condition, since the flow of the quark–gluon liquid adds to the pressure working against the vacuum; see section 3.5.

In Fig. 16.5, a similar discussion of the RHIC physical conditions is shown, following the same pattern as Fig. 16.4, except for the use of logarithmic scales. On the left-hand side, the energy range is now 10 GeV $\leq E/b \leq$ 190 GeV, and lines are in steps of 20 GeV. On the right-hand side, the specific entropy range is $50 \leq S/b \leq 500$, in step of 50 units. The lines become denser toward higher energy or entropy. The dotted lines in panels (c) and (f) indicate where the particle pressure is balanced by the vacuum pressure.

In the RHIC run at $\sqrt{s_{\rm NN}} = 130$ GeV, the final hadron phase space at central rapidity, the intrinsic local-rest-frame energy per baryon is $E/b \simeq 25$ GeV, while the entropy content is $S/b \simeq 150$, the uncertainties in both values are of 10%–15%, compare with table 19.4 on page 367. The exact

https://doi.org/10.1017/9781009290753.022 Published online by Cambridge University Press

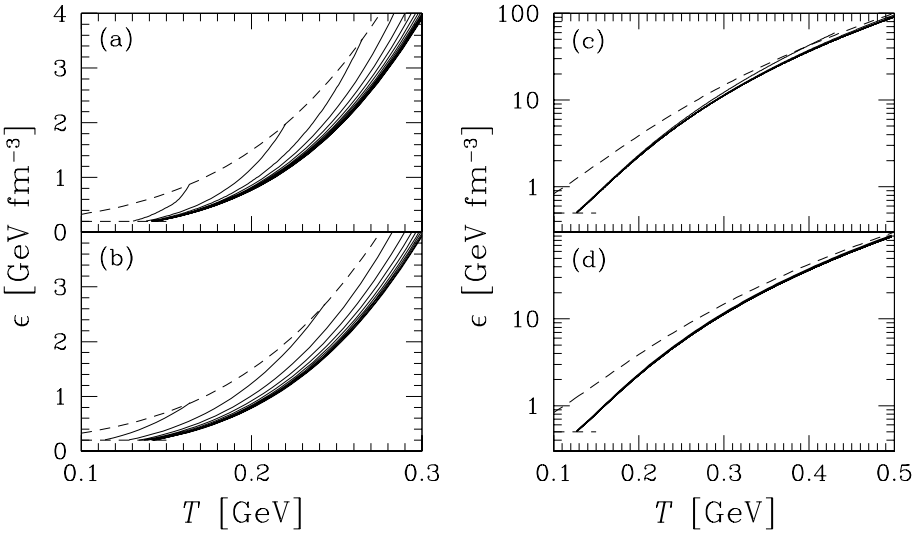

Fig. 16.6. The energy density as a function of temperature for a quark–gluon liquid. Top, at fixed E/b; bottom, at fixed S/b; left for the SPS and right for the RHIC energy domain. Limits are energy density $\epsilon = 0.5$ GeV fm^{-3} and baryo-chemical potential $\mu_{\rm b} = 1\,$GeV. Lines: left top for fixed $E/b = 2$ to 15 GeV in steps of 1 GeV; left bottom, at fixed $S/b = 10$ to 60 in steps of 5; right top, at fixed $E/b = 10$ to 190 GeV in steps of 20 GeV; and right bottom, at fixed $S/b = 50$ to 500 in steps of 50.

values of E/b and S/b depend on the way one accounts for the influence on the yield analysis of unresolved (at the time of writing) weak decays of hyperons and assumptions made about chemical equilibria. Despite this substantial increase compared to the energy and entropy content seen at the SPS, the value of $T_{\rm ch}$ consistent with this result is only 30–40 MeV higher than that at the SPS. For this reason, the increases in the particle multiplicity we have discussed in section 9.5 are relatively modest.

The rise of energy density with temperature at fixed E/b and S/b is shown in Fig. 16.6, for the expected domain of parameters at the SPS on the left and for the domain of RHIC parameters on the right; the lines follow the same key as that used in Figs. 16.4 and 16.5. We see the expected rise with T^4, but the narrow band of values associated with baryon content is quite striking. In fact, in the right-hand panel the different lines coalesce, energy density is effectively solely a function of T for $E/b > 10$ GeV and $S/b > 50$.

These results indicate clearly how the presence of baryon-rich quark matter possibly formed at lower collision energies augments the entropy and energy content. At large baryon density these results depend strongly

https://doi.org/10.1017/9781009290753.022 Published online by Cambridge University Press

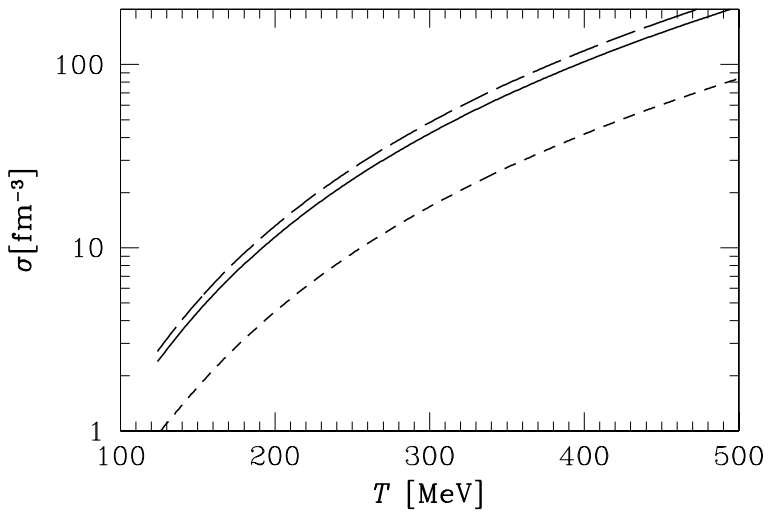

Fig. 16.7. The entropy density in chemically equilibrated QGP at $\lambda_q = 1$ as a function of temperature: solid line, $n_f = 2$; long-dashed line, $n_f = 2.5$; and short-dashed line, 'pure glue' $n_f = 0$.

on the validity of the extrapolation made from $\mu_b = 0$ of the quark–gluon liquid and there is no way to estimate the associated systematic error until lattice results of comparable quality for $\mu_b \neq 0$ become available. However, it would appear that at above $E/b > 3$ GeV, conditions suitable for formation of deconfined state are present.

Entropy plays a very important role in the study of scaling one dimensional hydrodynamic expansion, and the hadron yield in the final state offers a reliable measure of the product $\sigma_0\tau_0$, Eq. (7.27). In Fig. 16.7, the entropy density σ is shown as a function of temperature. The solid line is for the case of an equilibrated light-quark–glue system in the limit of vanishing chemical potential. We note that initially the entropy rises faster than the asymptotic T^3 behavior, since the quantum chromodynamics interactions weaken, and there is an increase in the effective number of acting quark and gluon degrees of freedom. Thus, the drop in entropy density on going toward the hadronization condition is considerable. In order to preserve the entropy content in the fireball when the QGP fireball expands, from $T \simeq 300$ MeV toward 150 MeV, a volume growth by a factor of nine must occur.

The 'pure-glue' case (short-dashed line) contains as expected about half of the entropy when one makes a comparison at equal temperature. The addition of strangeness expressed by increasing $n_f = 2$ to 2.5 adds about 10% to the entropy content.

https://doi.org/10.1017/9781009290753.022 Published online by Cambridge University Press